Histol Histopathol (2018) 33: 475-485

http://www.hh.um.es

Histology and Histopathology

From Cell Biology to Tissue Engineering

Automatic detection of DNA double strand breaks after irradiation using an γH2AX assay

Tim Hohmann[1]*, Jacqueline Kessler[2]*, Urszula Grabiec[1], Matthias Bache[2], Dirk Vordermark[2] and Faramarz Dehghani[1]

[1]Department of Anatomy and Cell Biology and [2]Department of Radiotherapy, Martin Luther University Halle-Wittenberg, Halle (Saale) Germany

*These authors contributed equally

Summary. Radiation therapy belongs to the most common approaches for cancer therapy leading amongst others to DNA damage like double strand breaks (DSB). DSB can be used as a marker for the effect of radiation on cells. For visualization and assessing the extent of DNA damage the γH2AX foci assay is frequently used. The analysis of the γH2AX foci assay remains complicated as the number of γH2AX foci has to be counted. The quantification is mostly done manually, being time consuming and leading to person-dependent variations. Therefore, we present a method to automatically analyze the number of foci inside nuclei, facilitating and quickening the analysis of DSBs with high reliability in fluorescent images.

First nuclei were detected in fluorescent images. Afterwards, the nuclei were analyzed independently from each other with a local thresholding algorithm. This approach allowed accounting for different levels of noise and detection of the foci inside the respective nucleus, using Hough transformation searching for circles.

The presented algorithm was able to correctly classify most foci in cases of "high" and "average" image quality (sensitivity>0.8) with a low rate of false positive detections (positive predictive value (PPV) >0.98). In cases of "low" image quality the approach had a decreased sensitivity (0.7-0.9), depending on the manual control counter. The PPV remained high (PPV >0.91). Compared to other automatic approaches the presented algorithm had a higher sensitivity and PPV.

The used automatic foci detection algorithm was capable of detecting foci with high sensitivity and PPV. Thus it can be used for automatic analysis of images of varying quality.

Key words: γH2AX, Hough transformation, Foci Segmentation, Foci Detection, Foci

Offprint requests to: Faramarz Dehghani, Institute of Anatomy and Cell Biology, Martin Luther University Halle-Wittenberg, Grosse Steinstrasse 52, 06108 Halle (Saale), Germany. e-mail: faramarz.dehghani@medizin.uni-halle.de

DOI: 10.14670/HH-11-945

Introduction

Radiotherapy belongs to the most common types of therapy for cancer (Ramaekers et al., 2011) leading to DNA damage in the irradiated cells. The DNA alterations appear in form of single strand breaks, double strand breaks and multiple other damage types, from which the double strand breaks are the most toxic form (van Gent et al., 2001) because these lesions are more complex and difficult to repair (Suzuki et al., 2003; Sancar et al., 2004). A typical way to visualize the scale of DNA damage is by labeling γH2AX, the phosphorylated form of the H2A histone protein variant which is part of the DNA damage signaling, located in very close proximity to DNA double-strand breaks (Rogakou et al., 1998; Rodrigue et al., 2006). It has also been shown that the number of formed γH2AX foci scales with the radiation dose (Rogakou et al., 1999; Sedelnikova et al., 2002; Riballo et al., 2004), making this staining a reliable target for visualizing DNA damage.

For evaluating the γH2AX foci assay manual counting has been reported as the method of choice in several studies (Vandevoorde et al., 2014; Brand et al., 2015; Nagy et al., 2016), but this approach is time consuming, cumbersome and subjective. To overcome these issues several (semi-) automated approaches have been introduced with varying degrees of success and complexity (MacPhail et al., 2003; Qvarnström et al., 2004; Böcker and Iliakis, 2006; Costes et al., 2006; Leatherbarrow et al., 2006; Mahrhofer et al., 2006; Marková et al., 2007; Cai et al., 2009; Hou et al., 2009; Roch-Lefèvre et al., 2010; Jucha et al., 2010; Ivashkevich et al., 2011; McVean et al., 2012; Neumaier et al., 2012; Runge et al., 2012). Most algorithms start with an optional noise filtering (Qvarnström et al., 2004; Böcker and Iliakis, 2006; Jucha et al., 2010; Ivashkevich et al., 2011), followed by an application of a top-hat filter (Qvarnström et al., 2004; Böcker and Iliakis, 2006; Jucha et al., 2010; Roch-Lefèvre et al., 2010; Ivashkevich et al., 2011), with a subsequent global thresholding (MacPhail et al., 2003; Qvarnström et al., 2004; Böcker and Iliakis, 2006; Leatherbarrow et al., 2006; Marková et al., 2007; Cai et al., 2009; Hou et al., 2009; Jucha et al., 2010; Roch-Lefèvre et al., 2010; Ivashkevich et al., 2011). Only few studies operated locally (Jucha et al., 2010; Ivashkevich et al., 2011; McVean et al., 2012). In several cases an object splitting algorithm has been applied to separate neighboring foci (Böcker and Iliakis, 2006; Cai et al., 2009; Ivashkevich et al., 2011; McVean et al., 2012; Neumaier et al., 2012). Besides these approaches there are fully automatic attempts that relied on image gradients and noise filters (Costes et al., 2006; McVean et al., 2012) or the analysis of foci in the wavelet domain using "à trous" wavelets (Neumaier et al., 2012). Still, the exact determination of foci numbers and characteristics remains complicated and error-prone, especially if image quality is varying.

Here we introduce an approach for foci detection that is based on the gradient image and considers the circular shape of foci using the Hough transformation. We furthermore compared the results of our approach with algorithms that were previously described by Böcker and Iliakis (Böcker and Iliakis, 2006), McVean et al. (2012) and Neumaier et al. (2012). We thereby observed that the presented approach significantly improves the evaluation, when compared to other automatic approaches.

Materials and methods:

Cell culture

Three different cell lines were used: U251 MG, LN229 and U343 MG. U251 MG and LN229 are primary glioblastoma cell lines (grade IV) and U343 MG is an anaplastic astrocytoma cell line (grade III). All cell lines were cultured in RPMI 1640 medium (Lonza, Walkersville, USA), supplemented with 10 % (v/v) fetal bovine serum (Thermo Scientific, Dreieich, DE), 1 % (v/v) sodium pyruvate (Thermo Scientific, Dreieich, DE), 185 u/ml penicillin and 185 μg/ml streptomycin (Biochrome, Berlin, DE).

Cells were left untreated (0 Gy) or irradiated with 2 Gy or 4 Gy 24 h before the fixation. Additionally, we irradiated LN229 cells with 2 Gy and fixed the cells 1 h after irradiation.

γH2AX assay

For γH2AX labeling cells were seeded in 8-well chambers (Thermo Scientific, Dreieich, DE). 24 hours after seeding, the cells were irradiated with 0 Gy (control group), 2 Gy or 4 Gy and cultured for another 24 h. Afterwards the cells were fixed for 10min with 4% paraformaldehyde (Sigma Aldrich, St. Louis, USA) and permeabilized with 0.5% Triton X-100 (Carl Roth, Karlsruhe, DE) /PBS (Lonza, Walkersville, USA) solution for 10 min, followed by a blocking step with 1% bovine serum albumin (Promega, Fitchburg, USA) for 1 h. Cells were then incubated with the phosphor-histone H2AX antibody (Cell Signaling, Danvers, MA, USA, dilution 1:400) and subsequently with the secondary antibody Anti-rabbit-Alexa 488 (Thermo Scientific, Dreieich, DE, dilution 1:400) for 1 h. For counterstaining of cell nuclei the cells were incubated for 5 min with DAPI (in PBS, 0.25 μg/μl; Carl Roth, Karlsruhe, DE).

Images were taken using an Axio Vert 200M (Carl Zeiss, Jena, DE) with a 63x objective, resulting in images with a resolution of 1388x1038 px, corresponding to 162.6x121.6 μm.

Detection of cell nuclei

Since fluorescence images were obtained, cell nuclei and foci could easily be separated using the rgb-color space. In the given case taking only the blue channel of the image separated nuclei from foci. Since the samples were not perfectly oriented in the focal plane of the microscope and the fluorescent labeling might be uneven a median filter and a contrast-limited adaptive histogram equalization algorithm were applied. Afterwards, a level set function, based on the Chan-Vese energy was used to identify cell nuclei (Song and Chan, 2002; Tai and Yao, 2006). Overlapping nuclei were split using a modified watershed approach (Zhang et al., 2012). The obtained nuclear boundaries were used to generate a rectangle defining the sub-image in the foci channel, were the foci detection was conducted.

Detection of foci

For foci detection the sub images defined by the nuclear regions were used, so that the used algorithm can be considered to act locally. First a morphological top hat filter was applied. Afterwards the image was transformed into a gradient magnitude image and a histogram of the gradient magnitude values was formed.

The gradient magnitude image G of a grayscale image I is obtained by calculating the Euclidean norm of the image gradient in x and y direction for each pixel:

$$G = \sqrt{\left(\left(\frac{\partial I}{\partial x}\right)^2 + \left(\frac{\partial I}{\partial y}\right)^2\right)}$$

The gradient magnitude image highlighted the boundaries of foci, facilitating the extraction. To get a reasonable threshold for transforming the gradient image into a binary, two approaches were used: the mean-value of the current gradient magnitude image and the k-means cluster algorithm applied to the histogram for two clusters. In the second case the threshold was considered to be the lowest value of the cluster with the higher mean value. The final threshold was than chosen to be the minimum of both approaches.

To identify foci inside the resulting binary image, we applied a Hough transformation for detecting circles, because of the circular shape of foci. The Hough transformation is a method for extracting features or geometric patterns in binary images. To successfully find geometric objects a parameter space was created. The parameter space had the dimensionality of the parametric form of the object to be detected. In the case of circles it was three dimensional: the center coordinates and the diameter of the circle. Each non-zero pixel in the binary image was than mapped onto the three dimensional parameter space by trying all possible combinations of parameters and incrementing the parameter space at these positions by one (Xie and Ji, 2002). The best fitting circles were the ones with the highest score in the parameter space. Using this approach the Hough transformation is intrinsically able to split overlapping objects, based on the peaks in the parameter space. To take into account the size of foci we considered circles to be foci only if they had a radius between 3 and 10 pixels, corresponding to 0.35 μm and 1.17 μm, respectively.

Evaluation of the influence of foci overlap

To evaluate the influence of foci overlap on the detection accuracy we used artificial images mimicking foci. The image size was adjusted by imitating typical nuclei sizes using the following edge dimensions: 100 px, 150 px, 200 px and 250 px. These sizes were chosen to resemble the area of small (100 px), medium sized (150 px and 200 px) and large (250 px) cell nuclei. The images were than filled with 1 to 100 circular foci with a diameter of 9 px, using a uniform distribution (Böcker and Iliakis, 2006). The used foci size corresponds to a manual estimate of the typical foci size in the analyzed images.

After the generation of the synthetic foci images they were analyzed and the results compared with the known number of foci.

Comparison of the proposed method for foci detection with existing ones

For the present study we compared the proposed method for automatic foci detection with three approaches published before (Böcker and Iliakis, 2006; McVean et al., 2012; Neumaier et al., 2012). Böcker and Iliakis (Böcker and Iliakis, 2006) applied a 3x3 average filter, followed by a 7x7 top hat filter and binarized the resulting image with a fixed threshold. Afterwards a watershed transform was used for the separation of overlapping foci.

Neumaier et al. (2012) used the product of "à trous" wavelet planes, applying a fixed threshold to the resulting image and separated foci with a watershed transform.

McVean et al. (2012) performed an analysis based on the application of an hessian operator, followed by an laplacian operator, a crimmins speckle filter and subsequent thresholding using the maximum entropy method. Afterwards, the resulting image was closed with a 3x3 kernel. As the mentioned study did object splitting only on the basis of confocal laser scanning image stacks, we used the watershed algorithm to split objects for our analysis.

We adjusted the size of each kernel to the resolution of the analyzed images of this study. All fixed thresholds were chosen in such a way that they produce best possible results, tested on sample nuclei. Additionally, all automatic detection approaches were compared to the manual counting.

Comparison of manually and automatically obtained foci numbers

The automated foci detection was compared with the results of manual counting by two independent researchers (counter 1 and counter 2). For comparison we analyzed the correlation between manual and automatic results and additionally calculated the sensitivity and positive predictive value (PPV) for the measurements (Fielding and Bell, 1997).

The sensitivity is defined as the ratio between true positive detections and the sum of true positive and false negative detections (Fielding and Bell, 1997):

$$\text{Sensitivity} = \frac{\text{true positive}}{\text{true positive} + \text{false negative}}$$

The sensitivity can be interpreted as the probability to detect a focus that has been found manually.

The PPV is defined as the ratio of true positive detections to the sum of true positive and false positive detection (Fielding and Bell, 1997).

$$\text{PPV} = \frac{\text{true positive}}{\text{true positive} + \text{false positive}}$$

This value can be interpreted as a measure for the likelihood that a positive detection is a true positive detection. For statistics and calculation of the used 95% confidence intervals of the PPV and sensitivity the Wilson score interval was used (Wilson, 1927).

Results

The detection of foci

All cell types and radiation doses were analyzed with the same set of parameters, for all tested methods. For validation and comparison of the manually and automatically obtained results 130 cell nuclei of LN229 cells 24 h after irradiation were analyzed.

Manual counting resulted in an average of 18.1 or 20.1 foci per nucleus for LN229 cells, depending on the counter. The extreme values per cell varied between 0 and 162 foci in one nucleus for manual counting. The automatic evaluation using the proposed method was in general more conservative than the manual counting and led to only a relatively low number of false positive

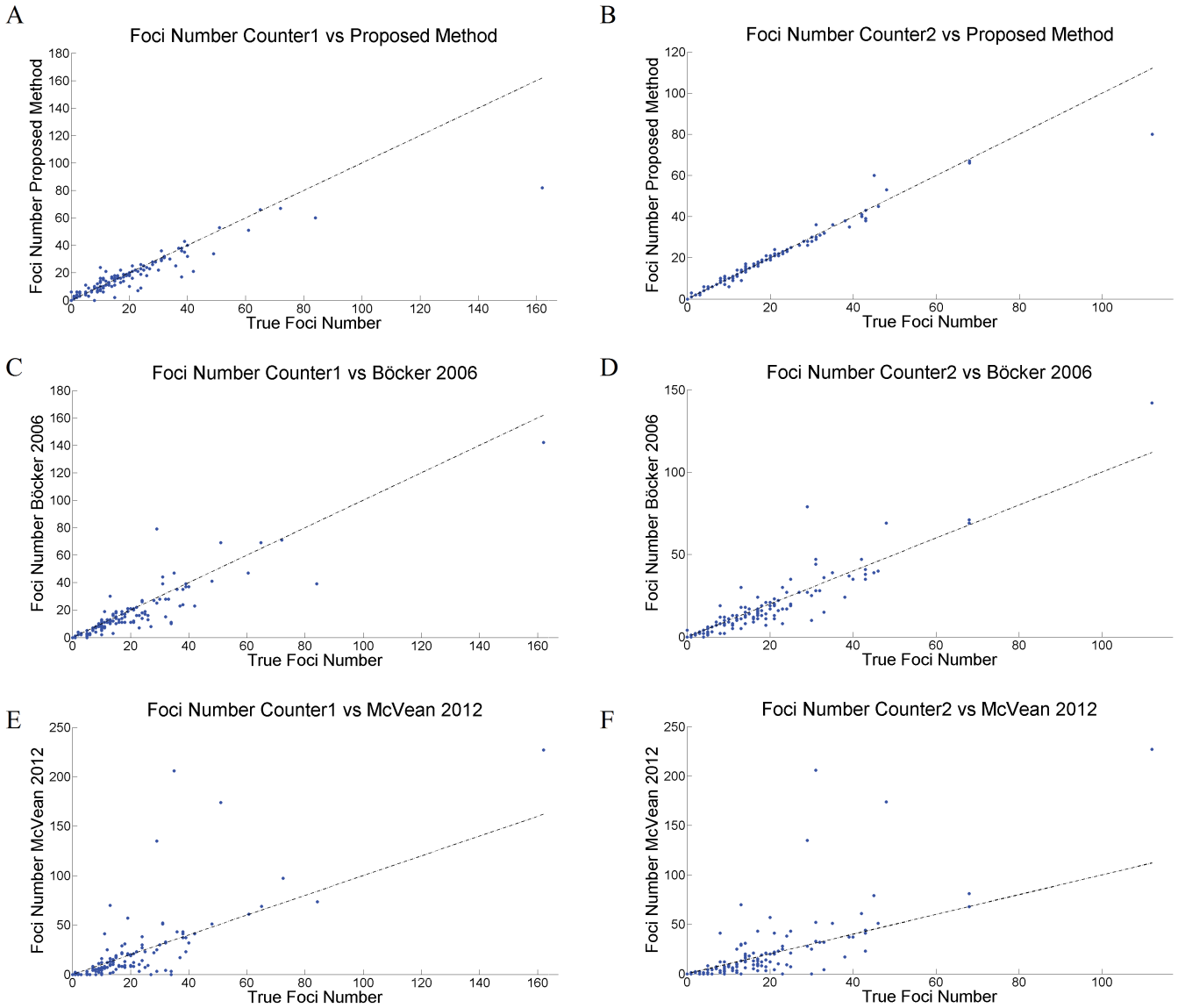

Fig. 1. Scatter plots of the results of manual and automatic foci counting using the proposed, Böcker and McVean algorithms for counters 1 **(A, C, E)** and 2 **(B, D, F)**. The black line depicts a line with slope 1 and offset of 0, corresponding to exact agreement between algorithmic and manual results. **A, B.** Show the results for the proposed method, which tends to slightly underestimate the foci number. **C, D.** Depict the result for the Böcker approach, which also tends to underestimate the foci number. **E, F.** Illustrate the results obtained after usage of the McVean method.

detection (below 5 %, Table 1).

After manual counting we compared our algorithm with the approaches proposed by Böcker and Iliakis (2006), Neumaier et al. (2012) and McVean et al. (2012). For the wavelet based method introduced by Neumaier et al., we could not get decent results (data not shown). We assume that the confocal laser scanning microscopy images used by Neumaier et al. (2012) for testing this algorithm were of considerably higher image quality, leading to the observed differences in foci extraction capability. Therefore, we did not include this method in the further analysis. A comparison of the number of observed foci per nucleus for the remaining methods showed that each method provides adequate results (Fig. 1, Table 1). Both the proposed method and the Böcker method tend to underestimate the number of foci (Fig. 1A-D, Table 1). A Pearson correlation analysis revealed for the proposed algorithm a value of r_1=0.913 [0.879;0.938] and r_2=0.976 [0.967;0.984] for the two counters. For the Böcker method it gave r_1=0.896 [0.855;0.925] and r_2=0.914 [0.879;0.938] and for the McVean method r_1=0.743 [0.654;0.812] and r_2=0.721 [0.625;0.795]. This implies, with regard to the given 95% confidence intervals, that the McVean method gave significantly different results from the other two

Table 1. Comparison of manual and automatic counting using the proposed, the Böcker 2006 and the McVean 2012 method for nuclei 24 h after irradiation.

	true positive	false negative	false positive
Counter1 Proposed	2279 (84.3%)	426 (15.7%)	76 (3.2%)
Counter1 Böcker2006	1963 (76.4%)	607 (23.6%)	248 (11.2%)
Counter1 McVean2012	1825 (71.2%)	739 (28.8%)	894 (32.9%)
Counter2 Proposed	2256 (95.6%)	105 (4.4%)	57 (2.5%)
Counter2 Böcker2006	1894 (81.7%)	425 (18.3%)	319 (14.4%)
Counter2 McVean2012	1689 (72.8%)	630 (27.2%)	1027 (37.8%)

The numbers in brackets denote the percentage of true positive and false negative detections relative to the overall numbers counted manually or the percentage of false positive signals relative to the overall number of detected foci by the respective algorithm.

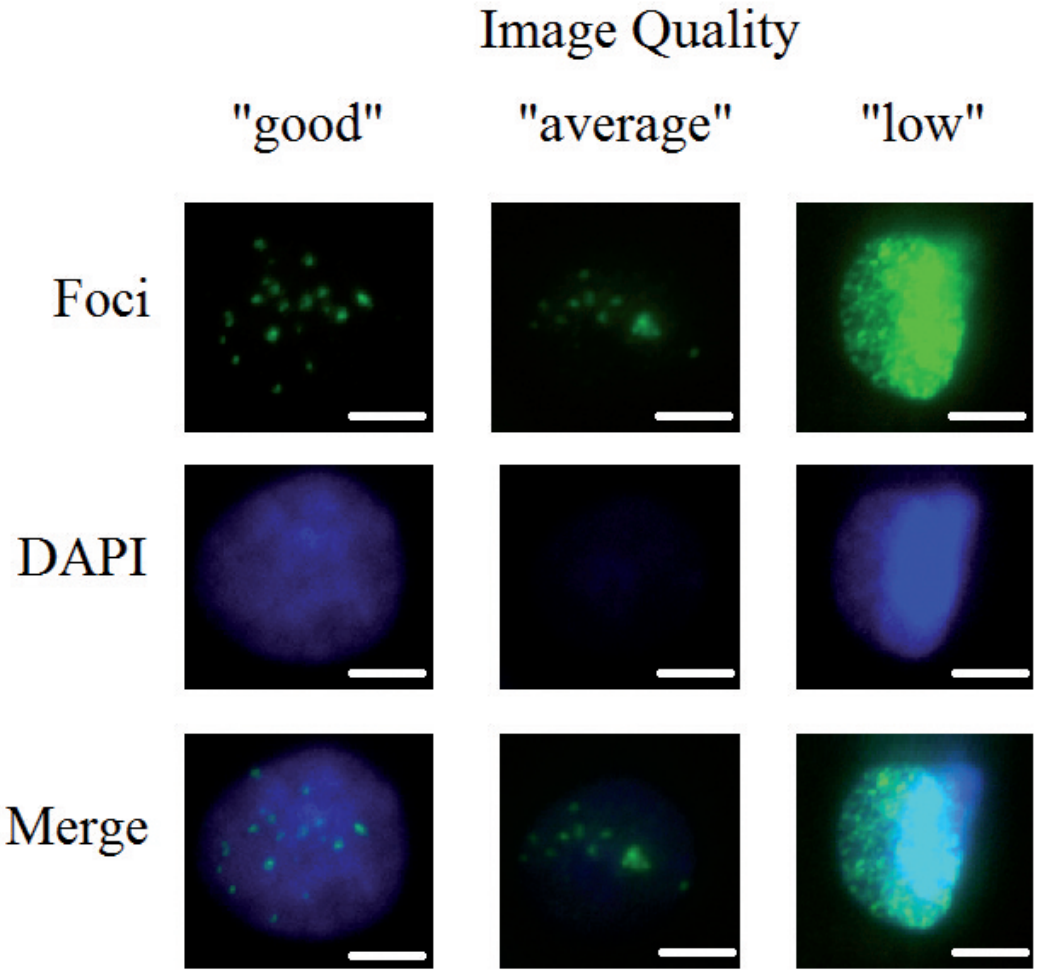

Fig. 2. Sample images of nuclei and the corresponding foci. Nuclei are shown in blue, while foci are labeled green. In a high quality image the foci signals are clearly distinguishable from the weakly labelled background. In case of an image with foci of "average" quality an increased background is visible when compared to the images of high quality. Foci overlap and are partially hard to distinguish from the background. Images of low quality illustrate foci that are in parts overexposed. Artefacts are visible, the background is comparably intense and individual foci are difficult to identify.
Scale bars: 5 μm.

approaches, while the proposed method and the Böcker approach gave comparable results with a slightly higher correlation for the proposed method.

A subsequent analysis of the sensitivity and PPV of all methods gave significantly better results for the PPV, when using the proposed method (Table 2). The sensitivity of the proposed method was 0.84 and 0.96 for counter 1 and counter 2, respectively. The Böcker method resulted in sensitivity values of 0.76 and 0.82, while McVeans approach led to 0.71 and 0.73. The PPV of the proposed method was for both counters larger or equal to 0.93, for the Böcker algorithm it was 0.89 and 0.86 and for McVean 0.67 and 0.62.

To identify what kind of images caused the differences in foci detection capabilities we grouped the foci images in three clusters corresponding to their image quality and ease of manual counting and calculated sensitivity and PPV for all algorithms for each group of images (Table 2). These groups were called, in accordance to the respective image quality, "good", "average" and "low", with group sizes of 56, 53 or 21 cell nuclei (Fig. 2). This grouping showed for the Böcker approach a decrease in PPV for images of low quality and an accompanying slight increase in sensitivity for counter 2 (Table 2). For the McVean method we observed an increase in sensitivity, with an accompanying strong decrease in PPV for images of low quality for both counters (Table 2). In contrast, the PPV of the proposed algorithm remained at a very high level (>0.93) and the sensitivity dropped moderately for counter 1 only (Table 2). Thus, images with a strong background, artefacts, varying foci intensity and size inside of one nucleus were the most critical parts in foci detection, especially for the approaches proposed by Böcker (Böcker and Iliakis, 2006) and McVean (2012) with a significantly lower PPV than the proposed method for images of "low" quality. The impact of those issues on the PPV of the proposed method for foci detection is significantly lower (Table 2; Fig. 3A).

As the highest foci number can be observed at approximately 1 h after irradiation, we additionally analyzed LN229 cells irradiated with 2 Gy after 1 h. We found an average of 25 and 20 foci per nucleus for 60 analyzed nuclei. The proposed algorithm was able to correctly identify most of the manually found foci (see Table 3, Fig. 4). Thereby, we observed a sensitivity that was virtually identical to the one observed 24 h after irradiation (0.84 and 0.98, see Table 4) and a slightly, but not significantly, reduced positive predictive value of 0.91 and 0.87 for the respective counter.

Reproduction of dose dependency

A further measure for validation of the used algorithm is the reproduction of known dose-response-relationships between radiation dose and foci number. In general, this behavior is characterized by a constant

Table 2. Comparison of manual and automatic counting in terms of sensitivity and PPV itemized to image quality for both counters and all 3 algorithmic approaches for nuclei 24 h after irradiation.

		Counter1 Proposed	Counter1 Böcker 2006	Counter1 McVean 2012	Counter 2 Proposed	Counter 2 Böcker 2006	Counter 2 McVean 2012
„All"	Sensitivity	0.84 [0.77,0.90]	0.76 [0.68,0.82]	0.71 [0.63,0.78]	0.96 [0.90,0.98]	0.82 [0.75,0.88]	0.73 [0.65,0.80]
	PPV	0.97 [0.94,0.99]	0.89 [0.82,0.93]	0.67 [0.59,0.74]	0.98 [0.95,0.99]	0.86 [0.79,0.91]	0.62 [0.53,0.70]
„Good"	Sensitivity	0.91 [0.81,0.96]	0.78 [0.65,0.87]	0.69 [0.56,0.80]	0.96 [0.87,0.98]	0.78 [0.66,0.87]	0.68 [0.55,0.78]
	PPV	0.95 [0.86,0.98]	0.93 [0.84,0.99]	0.85 [0.73,0.88]	0.99 [0.92,1.00]	0.95 [0.86,0.95]	0.86 [0.75,0.84]
„Average"	Sensitivity	0.84 [0.72,0.92]	0.78 [0.65,0.85]	0.67 [0.54,0.78]	0.94 [0.84,0.99]	0.81 [0.68,0.89]	0.70 [0.57,0.80]
	PPV	0.97 [0.89,0.99.]	0.96 [0.88,0.99]	0.79 [0.66,0.88]	0.99 [0.91,1.00]	0.89 [0.78,0.95]	0.74 [0.61,0.83]
„Low"	Sensitivity	0.75 [0.56,0.88]	0.70 [0.50,0.82]	0.80 [0.61,0.91]	0.97 [0.82,0.99]	0.91 [0.78,0.97]	0.89 [0.76,0.96]
	PPV	0.99 [0.85,1.00]	0.73 [0.53,0.84]	0.45 [0.28,0.63]	0.93 [0.82,0.98]	0.69 [0.49,0.81]	0.36 [0.2,0.55]

In Brackets the 95% confidence interval is given.

Table 3. Comparison of manual and automatic counting using the proposed method for nuclei 1 h after irradiation.

	true positive	false negative	false positive
Counter1	1245 (83.6%)	245 (16.4%)	120 (8.8%)
Counter2	1180 (97.7%)	28 (2.3%)	174 (12.9%)

The numbers in brackets denote the percentage of true positive and false negative detections relative to the overall numbers counted manually or the percentage of false positive signals relative to the overall number of detected foci by the proposed algorithm.

Table 4. Comparison of manual and automatic counting in terms of sensitivity and PPV for both counters and the proposed algorithm for nuclei 1 h after irradiation.

	Counter1	Counter 2
Sensitivity	0.84 [0.72,0.91]	0.98 [0.90,0.99]
PPV	0.91 [081,0.96]	0.87 [0.76,0.93]

In Brackets the 95% confidence interval is given.

slope for low and a sub linear increase for high doses. For this study U251 MG and U343 MG cells were left untreated (0 Gy) or irradiated with 2 or 4 Gy and the resulting foci numbers evaluated 24 h after irradiation. Therefore, 59, 85 or 56 U251 MG nuclei and 43, 35 or 33 U343 MG nuclei were analyzed after irradiation with 0, 2, or 4 Gy, respectively. Thereby for U251 MG cell nuclei, an average of 0.6 foci were found for control nuclei, 6.9 for 2 Gy and 11.8 for 4 Gy radiation. For U343 MG the foci numbers were 1.6, 6.2 and 10.4 for 0, 2 or 4 Gy, respectively (Fig. 3B). Thus, the linear dose-response-relationship is preserved.

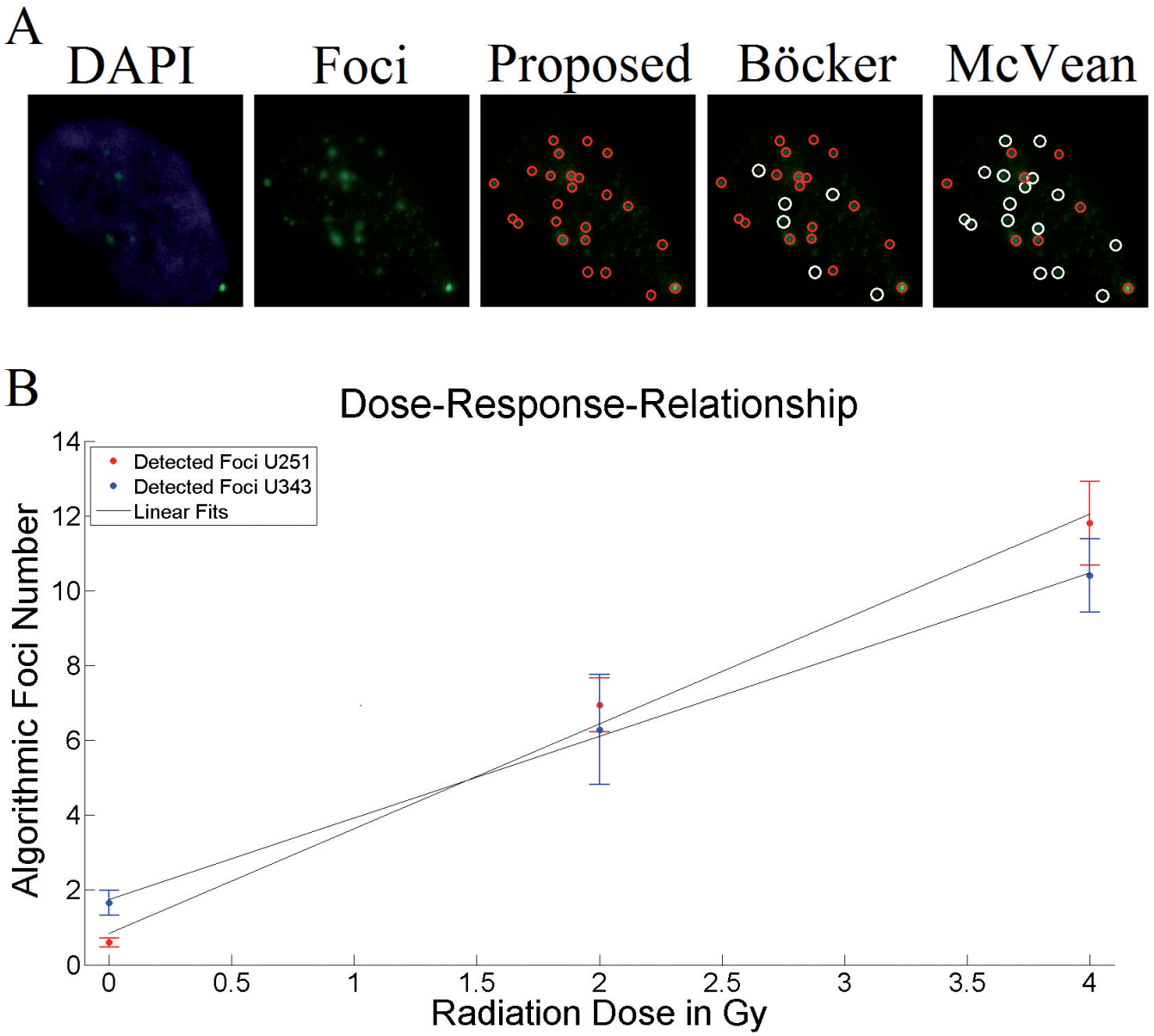

Fig. 3. Sample results for foci detection with the proposed, Böcker and McVean approach and dose-response-curve. **A.** Samples of nuclei labeled with DAPI and the respective foci, labelled with Alexa 488. In addition, the foci detection results for the proposed, Böcker and McVean method are marked with red circles. Missing detections, when compared to the manual counting, are displayed by white circles. The Böcker and McVean algorithms displayed a lower sensitivity due to the strongly varying foci intensity and size. For better visibility the contrast of the foci channel was enhanced using local contrast-limited adaptive histogram equalization. **B.** Results of foci detection after irradiation using the presented method. The foci detected for U251 MG (red) and U343 MG (blue) cells after irradiation with 0, 2 and 4 Gy with the respective standard error of the mean and linear fit in black are shown. The dose-response of both cell lines can well be approximated with a linear function, showing the capability of the proposed algorithm to reproduce linear dose-response relationships.

The influence of foci density on the actual foci count

For the evaluation of the effect of foci overlap synthetic images were generated for four different nuclei areas, with edge length of 100 px (small nucleus), 150 px (medium sized nucleus), 200 px (medium sized nucleus) and 250 px (large nucleus). For each nucleus size 100 images were generated and foci distributed inside the synthetic nucleus using a uniform distribution. Foci numbers from 1 to 100 were tested.

Thereby, the expected cell size dependent changes were observed in detection accuracy. Better results were found for larger nuclei, because of the lower foci density (Fig. 5). In addition, the point was calculated where the deviation between true foci number and detected foci number exceeded 10 % of the true foci number for the first time. Thereby, for small nuclei this point was reached for 17 foci, for medium-sized nuclei after 39 or 69 foci and for large foci the point was not reached for 100 foci. Calculating the area covered by foci inside the nuclei the transition point was roughly independent from the nucleus size and was reached when approximately 11 % of the nucleus was covered by foci. Thus foci overlap was an issue for nuclei with a high foci density only.

The non-linear shape of the curves should be considered as with increasing foci density the probability of high foci overlap rises because of the already occupied space by existing foci. As a result the probability of misdetection increases non-linearly.

Discussion

Here we present a method for automatic detection of γH2AX foci in labeled cells using standard fluorescence microscopy. To qualitatively characterize the used method, results from manual counting were compared to those obtained with the presented algorithmic results. In cases of "good" or "average" image quality the manual and automatic counting were almost equivalent, supporting the applicability of the used approach. Only for images of "low" quality were deviations from the manual counting found. In contrast, the PPV remained very high in all cases. In general, the automatic foci counting had several advantages compared to the manual counting, being its consistency, reproducibility, speed of analysis and non-existent biases. Automatic foci

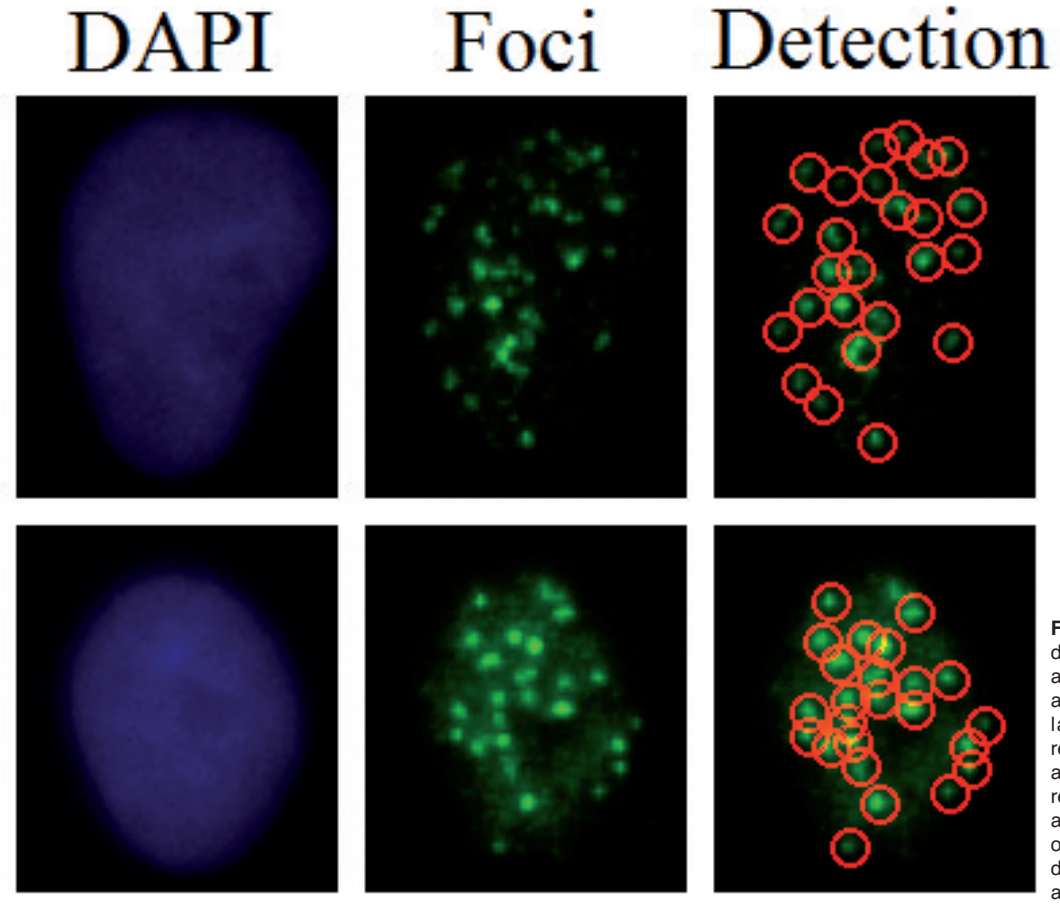

Fig. 4. Sample results for foci detection with the proposed approach for LN229 cells 1 h after irradiation. The nuclei are labeled with DAPI and the respective foci with Alexa 488. In addition, the foci detection results for the proposed method are marked with red circles. Most of the visible foci could be detected by the automatic approach.

identification allowed precise measurements of foci intensity and size, both being relevant parameters for foci evaluation (Cai et al., 2009).

Comparison of detection algorithms

Analyzing the algorithms reported in the literature has yielded different categories of approaches. One type consisted of setting a global threshold after image preprocessing with various noise filters and to count all remaining objects in the resulting binary image (MacPhail et al., 2003; Qvarnström et al., 2004; Leatherbarrow et al., 2006; Marková et al., 2007; Hou et al., 2009; Roch-Lefèvre et al., 2010). Other types used the same approach as before with an additional object splitting algorithm to identify overlapping foci (Böcker and Iliakis, 2006; Cai et al., 2009). Further approaches applied a local threshold after image pre-processing to identify foci (Jucha et al., 2010; Ivashkevich et al., 2011). Additionally, some authors used fully automatic attempts that relied on noise filtered gradient images (Costes et al., 2006; McVean et al., 2012) or the analysis of foci in the wavelet domain (Neumaier et al., 2012).

For all types of mentioned methods no comparison with the manual counting was made in terms of identity of the detected foci. The total number of foci was compared without determining the number of false positive and false negative foci. This approach might contain the risk of additional and thereby significant deviations of measured and real values. For the analysis of "morphological" features of foci (e.g. intensity, shape, size, position inside the nucleus etc.) this issue becomes even more severe.

Another point of interest, when comparing our approach to previously proposed algorithms, are algorithmic limitations. Most of the published approaches use global thresholds and thus neglect different background levels inside the cell nuclei, as well as size and shape constraints and all issues related to foci overlap (MacPhail et al., 2003; Qvarnström et al., 2004; Leatherbarrow et al., 2006; Marková et al., 2007; Hou et al., 2009; Roch-Lefèvre et al., 2010). Some authors used object splitting to address the issue of foci overlap (Böcker and Iliakis, 2006; Costes et al., 2006; Cai et al., 2009; Ivashkevich et al., 2011; McVean et al., 2012; Neumaier et al., 2012), but did not address the remaining difficulties. Several authors used local thresholding approaches, but neglected the shape and size of foci (Jucha et al., 2010; Ivashkevich et al., 2011). In contrast, the proposed algorithm considers all of these issues. Via the local thresholding different background levels can be considered. The Hough transformation not only allows accounting for the shape and size of foci, but is also intrinsically capable of splitting overlapping objects of similar shape.

Limitations of the foci detection method

The method presented here is generally capable of correctly identifying foci. Nevertheless, there are some restrictions that should be considered when the algorithm is applied. The first point concerns overlapping nuclei that cannot be separated. This results in the determination of foci numbers in multiple nuclei at once, leading to an inaccurate determination of local thresholds. As foci sometimes form dense clusters, object splitting remains also an issue in the foci image. Another study assigned large foci clusters a certain number of foci that was determined by the size of the cluster and typical foci size (Willitzki et al., 2013). A

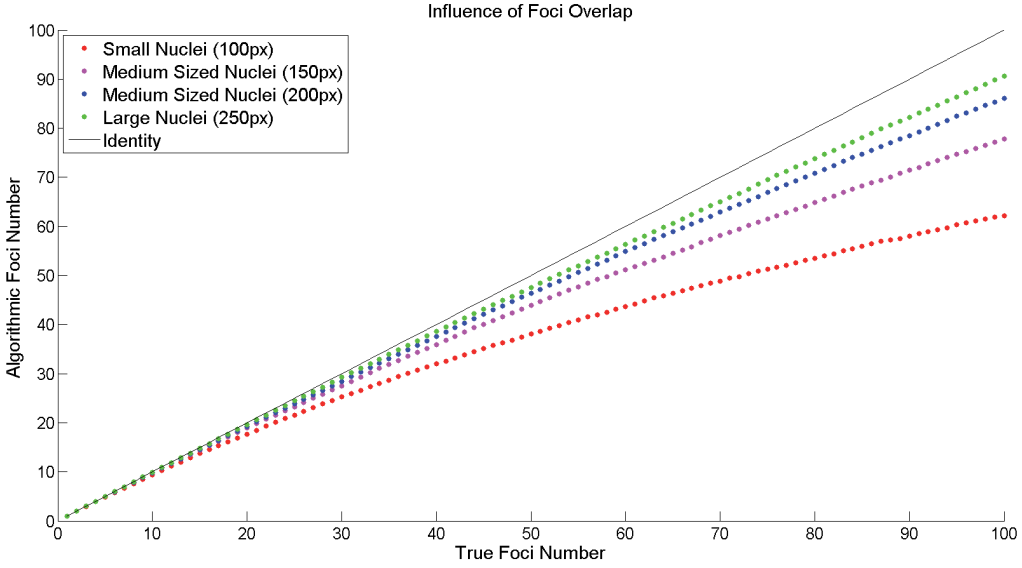

Fig. 5. Effect of foci overlap on the automatic detection of foci. Four synthetic nuclear sizes were generated as squares with edge length of 100-250 px, corresponding to small nuclei (100 px, red), medium sized nuclei (150 px, magenta and 200 px, blue) and large nuclei (250 px, green). For each nucleus size 100 images were created for each foci number from 1 to 100. The foci were uniformly distributed inside the synthetic nucleus. The true foci number is shown on the x-axis and the average detected foci number on the y-axis. The black line represents identical results for automatic detection and the true number of foci.

similar approach can be used here to assess foci clustering and improve the presented algorithm.

Additional improvement can be made by using confocal laser scanning microscopy or super-resolution microscopy. It further improves the signal to noise ratio and resolution, not only of the nuclei but also of the foci images, resulting in a better nucleus and foci segmentation. An adaption of the proposed algorithm to z-stacks is straight forward.

In summary, the presented foci detection algorithm is capable of automatically detecting foci with a high positive predictive value (PPV). Comparison with other automatic detection methods showed that the proposed method had a higher sensitivity and PPV. Thus, the used approach is suitable for analysis of images with varying quality, without the need of complex imaging methods. It furthermore facilitates the foci analysis and prevents manual biases.

References

Böcker W. and Iliakis G. (2006). Computational Methods for analysis of foci: validation for radiation-induced gamma-H2AX foci in human cells. Radiat. Res. 165, 113-124.

Brand M., Sommer M., Ellmann S., Wuest W., May M.S., Eller A., Vogt S., Lell M.M., Kuefner M.A. and Uder M. (2015). Influence of different antioxidants on X-ray induced DNA double-strand breaks (DSBs) using γ-H2AX immunofluorescence microscopy in a preliminary study. PLoS One 10, 1-12.

Cai Z., Vallis K.A. and Reilly R.M. (2009). Computational analysis of the number, area and density of gamma-H2AX foci in breast cancer cells exposed to (111)In-DTPA-hEGF or gamma-rays using Image-J software. Int. J. Radiat. Biol. 85, 262-271.

Costes S. V., Boissière A., Ravani S., Romano R., Parvin B. and Barcellos-Hoff M.H. (2006). Imaging features that discriminate between foci induced by high- and low-LET radiation in human fibroblasts. Radiat. Res. 165, 505-515.

Fielding A.H. and Bell J.F. (1997). A review of methods for the assessment of prediction errors in conservation presence / absence models. Environ. Conserv. 24, 38-49.

Hou Y.-N., Lavaf A., Huang D., Peters S., Huq R., Friedrich V., Rosenstein B.S. and Kao J. (2009). Development of an automated gamma-H2AX immunocytochemistry assay. Radiat. Res. 171, 360-367.

Ivashkevich A.N., Martin O.A., Smith A.J., Redon C.E., Bonner W.M., Martin R.F. and Lobachevsky P.N. (2011). Gamma-H2AX foci as a measure of DNA damage: A computational approach to automatic analysis. Mutat. Res. - Fundam. Mol. Mech. Mutagen. 711, 49-60.

Jucha A., Wegierek-Ciuk A., Koza Z., Lisowska H., Wojcik A., Wojewodzka M. and Lankoff A. (2010). FociCounter: A freely available PC programme for quantitative and qualitative analysis of gamma-H2AX foci. Mutat. Res. - Genet. Toxicol. Environ. Mutagen. 696, 16-20.

Leatherbarrow E.L., Harper J. V., Cucinotta F.A. and O'Neill P. (2006). Induction and quantification of gamma-H2AX foci following low and high LET-irradiation. Int. J. Radiat. Biol. 82, 111-118.

MacPhail S.H., Banáth J.P., Yu T.Y., Chu E.H.M., Lambur H. and Olive P.L. (2003). Expression of phosphorylated histone H2AX in cultured cell lines following exposure to X-rays. Int. J. Radiat. Biol. 79, 351-358.

Mahrhofer H., Bürger S., Oppitz U., Flentje M. and Djuzenova C.S. (2006). Radiation induced DNA damage and damage repair in human tumor and fibroblast cell lines assessed by histone H2AX phosphorylation. Int. J. Radiat. Oncol. Biol. Phys. 64, 573-580.

Marková E., Schultz N. and Belyaev I.Y. (2007). Kinetics and dose-response of residual 53BP1/gamma-H2AX foci: co-localization, relationship with DSB repair and clonogenic survival. Int. J. Radiat. Biol. 83, 319-329.

McVean A., Kent S., Bakanov A., Hobbs T. and Anderson R. (2012). Development and validation of "AutoRIF": software for the automated analysis of radiation-induced foci. Genome Integr. 3, 1.

Nagy Z., Kalousi A., Furst A., Koch M., Fischer B. and Soutoglou E. (2016). Tankyrases promote homologous recombination and check point activation in response to DSBs. PLOS Genet. 12, e1005791.

Neumaier T., Swenson J., Pham C., Polyzos A., Lo A.T., Yang P., Dyball J., Asaithamby A., Chen D.J., Bissell M.J., Thalhammer S. and Costes S.V. (2012). Evidence for formation of DNA repair centers and dose-response nonlinearity in human cells. Proc. Natl. Acad. Sci. USA 109, 443-448.

Qvarnström O.F., Simonsson M., Johansson K.-A., Nyman J. and Turesson I. (2004). DNA double strand break quantification in skin biopsies. Radiother. Oncol. 72, 311-317.

Ramaekers B.L.T., Pijls-Johannesma M., Joore M.A., van den Ende P., Langendijk J.A., Lambin P., Kessels A.G.H. and Grutters J.P.C. (2011). Systematic review and meta-analysis of radiotherapy in various head and neck cancers: Comparing photons, carbon-ions and protons. Cancer Treat. Rev. 37, 185-201.

Riballo E., Kuhne M., Rief N., Doherty A., Smith G.C.M., Recio M.J., Reis C., Dahm K., Fricke A., Krempler A., Parker A.R., Jackson S.P., Gennery A., Jeggo P.A. and Löbrich M. (2004). A pathway of double-strand break rejoining dependent upon ATM, Artemis, and proteins locating to γ-H2AX foci. Mol. Cell 16, 715-724.

Roch-Lefèvre S., Mandina T., Voisin P., Gaëtan G., Mesa J.E.G., Valente M., Bonnesoeur P., García O., Voisin P. and Roy L. (2010). Quantification of gamma-H2AX foci in human lymphocytes: a method for biological dosimetry after ionizing radiation exposure. Radiat. Res. 174, 185-194.

Rodrigue A., Lafrance M., Gauthier M.-C., McDonald D., Hendzel M., West S.C., Jasin M. and Masson J.-Y. (2006). Interplay between human DNA repair proteins at a unique double-strand break in vivo. EMBO J. 25, 222-231.

Rogakou E.P., Boon C., Redon C. and Bonner W.M. (1999). Megabase chromatin domains involved in DNA double-strand breaks in vivo. J. Cell Biol. 146, 905-916.

Rogakou E.P., Pilch D.R., Orr A.H., Ivanova V.S. and Bonner W.M. (1998). DNA Double-stranded Breaks Induce Histone H2AX Phosphorylation on Serine 139. J. Biol. Chem. 273, 5858-5868.

Runge R., Hiemann R., Wendisch M., Kasten-Pisula U., Storch K., Zöphel K., Fritz C., Roggenbuck D., Wunderlich G., Conrad K. and Kotzerke J. (2012). Fully automated interpretation of ionizing radiation-induced γH2AX foci by the novel pattern recognition system AKLIDES®. Int. J. Radiat. Biol. 88, 439-447.

Sancar A., Lindsey-Boltz L.A., Unsal-Kaçmaz K., Linn S., Ünsal-Kaçmaz K. and Linn S. (2004). Molecular mechanisms of mammalian DNA repair and the DNA damage checkpoints. Annu. Rev. Biochem. 73, 39-85.

Sedelnikova O.A., Rogakou E.P., Panyutin I.G. and Bonner W.M. (2002). Quantitative detection of 125 IdU-induced DNA double-

strand breaks with γ - H2AX antibody IdU-induced DNA double-strand breaks with γ -H2AX antibody. Radiat. Res. 158, 486-492.

Song B. and Chan T. (2002). A fast algorithm for level set based optimization. Cam-Ucla. 68, 1-20.

Suzuki K., Ojima M., Kodama S. and Watanabe M. (2003). Radiation-induced DNA damage and delayed induced genomic instability. Oncogene 22, 6988-6993.

Tai X.-C. and Yao C.-H. (2006). Image segmentation by piecewise constant {M}umford-{S}hah model without estimating the constants. J. Comput. Math. 24, 435-443.

van Gent D.C., Hoeijmakers J.H. and Kanaar R. (2001). Chromosomal stability and the DNA double-stranded break connection. Nat. Rev. Genet. 2, 196-206.

Vandevoorde C., Franck C., Bacher K., Breysem L., Smet M.H., Ernst C., De Backer A., Van De Moortele K., Smeets P. and Thierens H. (2014). γ-H2AX foci as in vivo effect biomarker in children emphasize the importance to minimize x-ray doses in paediatric CT imaging. Eur. Radiol. 25, 800-811.

Willitzki A., Lorenz S., Hiemann R., Guttek K., Goihl A., Hartig R., Conrad K., Feist E., Sack U., Schierack P., Heiserich L., Eberle C., Peters V., Roggenbuck D. and Reinhold D. (2013). Fully automated analysis of chemically induced γH2AX foci in human peripheral blood mononuclear cells by indirect immunofluorescence. Cytom. Part A. 83, 1017-1026.

Wilson E. (1927). Probable inference, the law of succession, and statistical inference. J. Am. Stat. Assoc. 22, 209-212.

Xie Y. and Ji Q. (2002). A new efficient ellipse detection method. Proceedings. 16th Int. Conf. Pattern Recognition, 2002. 2, 957-960.

Zhang C., Pham T.D., Sun C. and Su R. (2012). Segmentation of clustered nuclei based on curvature weighting categories and subject descriptors. ACM. 49-54.

Accepted November 15, 2017